Through-the-Multilayered Wall Imaging Using Passive Synthetic Aperture Radar

Hajar Abedi and Bijan Zakeri, *Member, IEEE*

***Abstract*— Most of the existing through-the-wall imaging (TWI) methods using synthetic aperture radar (SAR) tend to apply an active system. In this paper, a novel, passive SAR (PSAR), termed TWI-PSAR, is proposed, to focus the image of multi targets behind a single-/multilayered wall. TWI-PSAR would work in a bistatic configuration using wideband sources of opportunity and a single moving platform or a stationary linear array receiver. Incident angle and frequency are considered the parameters that influence TWI image directly. A stepped frequency transmitter with single incident angle is applied to investigate the incident angle effect. It could show the capability of small angle to suppress wall effects. Zero incident angle PSAR (Z-PSAR) is exploited in TWI for enhanced target identification and feature extraction as well as wall effect mitigation. In scenarios where background measurement might not be available or wall parameters are unknown for compensation, Z-PSAR could be adopted. Compared to other conventional imaging methods such as SAR and time reversal, numerical results show the superiority of the proposed TWI system in urgent situations with unknown wall parameters, employing free-space Green's function. Moreover, to demonstrate the effectiveness of the proposed PSAR method in a real situation, sources of opportunity that are relatively wideband and aligned in several directions, such as analog TV, Digital Video Broadcasting—Terrestrial, GSM, and WiMAX, are used to image targets behind the wall. Also, Monte Carlo method is used to show the effectiveness of TWI-PSAR in different frequency and incident angle scenarios.**

***Index Terms*— Background subtraction, passive synthetic aperture radar (PSAR), synthetic aperture radar (SAR), through-the-wall imaging (TWI), wall compensation, zero incident angle PSAR (Z-PSAR).**

I. Introduction

PROPAGATION of electromagnetic waves through walls has received much interest in terms of wireless communication devices, becoming omnipresent nowadays. Through-the-wall imaging (TWI) has received considerable attention in research and engineering community. Operating radar in low-frequency microwave range has the advantage of good penetration into building structures. UWB excitation and synthetic aperture radar (SAR) technologies could be employed in order to obtain good range and cross-range resolution [1]–[3].

Manuscript received February 26, 2018; revised June 30, 2018 and November 12, 2018; accepted December 12, 2018. *(Corresponding author: Bijan Zakeri.)*

The authors are with the Electrical Engineering Department, Babol Noshirvani University of Technology, Babol 47148-71167, Iran (e-mail: zakeri@nit.ac.ir).

Color versions of one or more of the figures in this paper are available online at http://ieeexplore.ieee.org.

Digital Object Identifier 10.1109/TGRS.2018.2890027

Recently, TWI using SAR (TWI-SAR) has nearly entered a stage of technological maturity. Most of the TWI-SAR techniques have been based on monostatic cases, with both transmitter and receiver being onboard the same platform [4]–[7]. In the last two decades, intensive studies have been carried out on bistatic and multistatic radar observations to image the target behind a wall [8], [9]. The main advantage of such a configuration is that a target can be observed from different bistatic angles, providing more information about the target [10]. Using an active antenna as transmitting sources is common in TWI studies. A further step in bistatic radar development is to use transmitters of opportunity for scene illumination instead of dedicated and easily detected SAR transmitters. This would lead directly to the idea of passive SAR (PSAR) imaging. The emergence in recent years of digital communication technologies, such as WiFi, DAB, and Digital Video Broadcasting—Terrestrial (DVB-T), has stimulated research in the passive radar field to identify applications which exploit these new transmitters of opportunity. The receive-only nature of passive systems enables them to be of low cost, widely deployable, undetectable, low power consumption, and potential ability to detect stealth targets, due to the multistatic geometry [11]–[14].

While many of PSARs have focused on airborne [13]–[16], in this paper, PSAR is utilized to detect objects behind a single- or multilayered wall, comprising far-field transmitters, with receivers located near the wall. The idea is applied to TWI scenarios with full-wave finite-difference time domain (FDTD) numerical electromagnetic simulations with a plane wave transmitter as a source of opportunity.

It is well-understood that in TWI, in order to compute the image, an efficient evaluation of the wall medium Green's function, a time consuming and complicated process, is required [23]. Although extensive research has been conducted in the term of medium Green's function regardless of the estimated value of the wall parameters [17], [18], wall parameter estimation is a prerequisite for many conventional TWI methods. In other words, one of the main drawbacks of such techniques, monostatic SAR, and time reversal, for example, is known to be the essential need of background subtraction and wall compensation.

Several methods were proposed to reduce the adverse effects of wall reflection, resulting in masking target image. In [19], wall EM returns were mitigated in TWI using singular value decomposition. Spatial filters across the antenna array [20] were applied to remove, or at least significantly mitigate,

the spatial zero-frequency and low-frequency components which correspond to wall reflections. Frequency-modulated interrupted continuous wave signals was proposed in [21] as a wall removal technique. In [22], the image formation was based on differential SAR image formation employing a continuous-wave radar system. In this approach, instead of using individual backscattered signals, the image was formed by employing the difference signals obtained by subtracting two successive signals along the track. Polarimetric imaging [6], [7], [23] could be another wall mitigation technique which not only enhances the target characterization but also mitigates the wall ringing effect in cross polarizations. Although without background subtraction, successful imaging results could be obtained using these algorithms, they would mainly deal with wall compensation scenarios which necessitate wall parameters to be known. This problem tends to be more pronounced in the presence of multilayered walls.

In this paper, due to the fact that the illuminator of opportunity is considered a plane wave and the incident angle of transmitters would directly affect target images behind walls [2], a single (1–3 GHz) stepped-frequency transmitter of opportunity aligned in various angles is considered to investigate angle effects of transmitters. It is shown that a stepped frequency transmitter with a single incident angle could be applied to eliminate the essential need for background subtraction and wall compensation. Moreover, in the case of zero angel, due to the minimum reflection from the wall, it could be indicated that zero incident angle PSAR (Z-PSAR) would not only mitigate wall reflection effects, but, in conjunction with monostatic SAR images, provide more detailed information of targets without using wall compensation method. Consequently, wall parameters would not be essential to be known in Z-PSAR method. Meanwhile, a comparison between the TWI-PSAR, SAR and time reversal method (TRM) [28] in terms of the capability of detection/imaging without background subtraction and wall compensation is also made. It specifies the superiority of TWI-PSAR in detection and imaging by applying free-space medium Green's function. Furthermore, for sensitivity analysis of the proposed TWI system, a new parameter termed signal-to-wall ratio (SWR) is defined to compute the capability of wall direct signal suppression.

It should be pointed out that wave velocity differences between free space and the wall would lead to detecting the target, relatively farther away from its actual location. Consequently, this method shows better to be used in urgent conditions, such as earthquakes when the speed of detection would play a key role.

In addition, to show the effectiveness of PSAR in a real situation, sources of opportunity known to be relatively wideband, such as analog TV, DVB-T, GSM, and WiMAX, located randomly, are used to image targets behind a wall. Besides, to evaluate the TWI-PSAR performance in the presence of other sources, with different frequency and incident angle, Monte Carlo method is used. Since not all of these transmitters would illuminate the target with single incident angle, wall effect needs to be compensated. Thus, a generalized Green's function-based approach for imaging the targets behind a wall [23] is incorporated for the compensation of the wall effects.

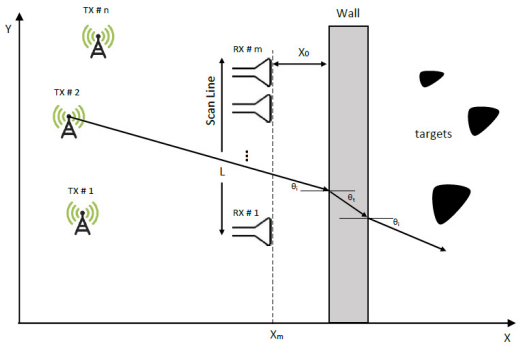

Fig. 1. Geometry of TWI-PSAR system.

Hence, the proposed TWI-PSAR method could play crucial role in urgent situations. A wideband source of opportunity with a single angle could be utilized for the elimination of direct reflections from the wall. Also, the Z-PSAR tend to eliminate the need for wall parameters estimation and wall mitigation/ compensation, leading to an increased SWR. Furthermore, in the absence of a wideband source, several transmitters with different frequencies can cooperate in order to make a wideband transmitter and to image a target with a proper resolution. This paper is organized as follows: In Section II, the concept of passive SAR in TWI is introduced. In Section III, standard SAR imaging technique and compensation methods for refocusing behind the wall are formulated. Some numerical results are provided in Section IV. Finally, the conclusion is drawn in Section V.

II. Concept of TWI-PSAR System

The rapid growth in the number of RF emissions for TV and radio broadcasts in addition to terrestrial- and space-based communications has resulted in a wide range of signal types available for exploitation by passive radar. Furthermore, the receive-only nature of passive systems enables them to be of low cost, widely deployable, undetectable, low power consumption, and potential ability to detect stealth targets, due to the multistatic geometry. Multistatic SAR could simultaneously provide multiple SAR images with different viewing geometries, thereby increasing the observation space considerably. This facilitates the detection, classification, and recognition of objects. These features of passive radar make it the suitable and attractive sensor for TWI that would yield very effective results, particularly in urgent conditions, such as earthquakes when the speed of detection would play a crucial role in the absence of active source.

A new passive system in TWI would comprise a plane wave transmitter of opportunity together with a receiver located near the target. The receiver could be mounted on a moving platform or fixed as an array antenna (linear array for strip-map mode). The system is presented in Fig. 1. In TWI, it is possible to use multiple receivers with a single wideband illuminator, or indeed several illuminators, allowing multistatic configurations. TWI-PSAR systems can be operated in different configurations. One of the configurations tends to use a passive

receiver mounted on the moving platform, utilizing stationary illuminators of opportunity. Opposite mode can also be distinguished, with the illuminator being placed on moving platforms, such as aircraft and satellite with stationary receivers.

In passive imaging, appropriate transmitters would be selected due to proper bandwidth and beamwidth. Direction could be estimated suing ELINT systems [24]. In general, passive systems can use different types of sources to illuminate targets. In TWI, an illuminator with a bandwidth of 1–1.5 GHz at UHF to low microwave frequencies, to provide the required range resolution, and reasonable power are required. Cross-range resolutions, on the other hand, are obtained by synthetic apertures or linear array of receiver. However, it may not be possible to find a single source of opportunity with at least 1-GHz bandwidth. A wideband transmitter can also be obtained by coherently adjoining several existing illuminators. Assuming the desired power density, DAB radio, DVB-T television, GSM mobile system, and Wi-Fi are considered valuable resources in TWI-PSAR with at least two advantages. First, they are abundant, and the second, their operating frequency is appropriate for propagation through walls. However, in a real transmission environment, many data signals would also be present in addition to the beacon signal.

The greatest limitation of bistatic radar performance would be the presence of directly transmitted signals [14]. In TWI, wall direct reflection is considered to be significant. Therefore, to create a good quality image, it seems necessary to remove wall reflection and direct signal from the transmitter. It is prevalent to use a directive antenna in TWI [2] which itself would mitigate the direct signals. In other words, directive receiver, Horn, for instance, would collect very small ratio of transmitter signals. In the case where the receivers are directed toward targets and wall, the direct signal to echo signal ratio would decrease. The remaining direct power, which might still mask the weak signals, can be further removed using CLEAN techniques [25], [26]. The application of this procedure reduces the direct signals, which significantly decreases the masking effect and improves the final PSAR-TWI image. In the proposed TWI-PSAR system, it was assumed as follows.

1) Receiver is located between the source of illumination and targets, shown in Fig. 1.
2) Receiver antenna is directed toward the wall and targets so it just has the capability of receiving reflected signals from the wall and targets. Direct-path signals from the transmitter will not be collected by the receiver.
3) All of the available transmitters of opportunity emit plane wave.
4) Location and direction of each transmitter are known. As illustrated in Fig. 1, the incident angle is the angle between a wave incident on the wall and the line perpendicular to the wall at the point of incidence, called normal.

III. Problem Formulation

In Fig. 1, a simple scenario of target detection behind multilayered walls using PSAR is presented. With a far-field assumption, single or multitransmitters emitted a signal, and the receiver antenna, stationary linear array, or a single antenna moving along scan line could collect scattered fields at different frequency and observation points. The scan line is chosen to be parallel to the wall, located at x_m. The return signal at the receiver is then coherently processed using TWI algorithms to form a focused image of targets. Under the point target model, ignoring multiple scattering effects, the received signal could be written as [23]

$$E_s(r_{rm}, r_{tn}, k_p) = \int G(r_{rm}, r, k_p) G(r, r_{tn}, k_p) \sigma(r) dr \quad (1)$$

where $E_s(r_{rm}, r_{tn}, k_p)$ is the received scattered field from the target at mth receiver location due to illumination of nth transmitter, σ is the reflectivity of the target, and r_{tn}, r_{rm}, and r are position vectors of nth transmitter, mth receiver and the target, i.e., $r_{tn}(x_{tn}, y_{tn})$, $r_{rm}(x_{rm}, y_{rm})$, and r (x,y), and k_p is the freespace wavenumber of pth operating frequency, $G(r, r_{tn}, k_p)$ and $G(r_{rm}, r, k_p)$ are medium Green's functions which relate the wave propagation process from the transmitter to the target and from the target to the receiver in the presence of the wall. Given the received signal at all antenna locations, the image could then be created as

$$I(r) = \sum_{m=1}^{M} \sum_{n=1}^{N} \sum_{p=1}^{P} E_s(r_{rm}, r_{tn}, k_p) \times G^{-1}(r, r_{rm}, k_p) G^{-1}(r, r_{tn}, k_p) \quad (2)$$

where P is the total number of frequencies. With a far-field assumption, to compromise between the computation efficiency and the accuracy, the standard focused SAR imaging technique would be

$$I(r) = \sum_{m=1}^{M} \sum_{n=1}^{N} \sum_{p=1}^{P} E_s(r_{rm}, r_{tn}, k_p) e^{jkp(R_{tn}+R_{rm})} \quad (3)$$

and the TWI could then be reconstructed as

$$I(r) = \sum_{m=1}^{M} \sum_{n=1}^{N} \sum_{p=1}^{P} E_s(r_{rm}, r_{tn}, k_p) e^{jkp(R_{tn}+R_{rm})} \times (T_r(r, r_{rm}, k_p) T_t(r, r_{tn}, k_p))^{-1} \quad (4)$$

where $R_{tn} = |r_{tn} - r|$, $R_{rm} = |r_{rm} - r|$, T_t and $\mathrm{T_r}$ are wall transmission coefficients from the transmitter to target and the target to receiver, respectively. Wall transmission and reflection coefficient, i.e., T and Γ, for single-layered wall could be derived as [2], [27]

$$T_{\upsilon/h} = \frac{4e^{i(k_{1x}-k_{0x})d}}{(1+p_{01})(1+p_{10})\left(1+R_{01}R_{10}e^{i2k_{1x}d}\right)}$$
$$\Gamma_{\upsilon/h} = \frac{\left(R_{01}+R_{10}e^{i2k_{1x}d}\right)}{\left(1+R_{01}R_{10}e^{i2k_{1x}d}\right)} \quad (5)$$
$$p_{01} = \frac{1}{p_{10}}, \quad R_{10} = -R_{01} = \frac{1-p_{01}}{1+p_{01}}$$
$$k_{0x} = k_p \cos(\theta_i) \quad k_{1x} = k_p \sqrt{\varepsilon_r} \cos(\theta_t) \quad (6)$$

where $p_{10} = k_{0x}/k_{1x}$ is for h polarization, and $p_{10} = \varepsilon_r k_{0x}/k_{1x}$ for υ polarization of the incident field. In (6), ε_r is relative dielectric constant, d is the thickness of the wall, and k_{0x} and k_{1x} are normal components of propagation constants in the air and dielectric, respectively. Furthermore, θ_i and θ_t

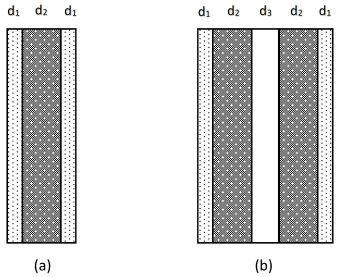

Fig. 2. Geometry of multilayered wall. (a) Three layers. (b) Five layers.

TABLE I
THREE-LAYERED WALL PARAMETERS

Layers	type of layer	permittivity (ε)	conductivity σ (s/m)	thickness (cm)
1st layer	concrete	6.8	0.1	3
2nd layer	brick	2.3	0.03	10
3rd layer	concrete	6.8	0.1	3

are the incident angle in the air and dielectric. More detailed information about computation of transmission coefficient of multilayered could be seen in [7]. For the target signal in TWI, the major problem tends to be the strong direct signal from the wall that would also be received by the target echo antenna. In other words, wall would act as a clutter. It seemed clearly vital to reduce this direct signal to minimize target-masking effects. To show the capability of wall direct signal suppression in TWI-PSAR systems, a new parameter termed SWR was defined as

$$\mathrm{SWR} = 10\log\left(\frac{P_s}{P_w}\right) \tag{7}$$

where P_s and P_w are the power of the signal and wall, respectively.

IV. NUMERICAL RESULTS

From (5) and (6), the transmissivity matrix could be a function of both frequency and angle. Regardless of power density in TWI-PSAR, both parameters would have strong impacts on a through-the-wall target image. Several sets of numerical simulations were presented in three subsections to analyze the effect of both parameters, in single-/multilayered wall scenarios. The scattering signal from the wall and the target was simulated using a time domain 2-D full wave EM solver based on FDTD method. Then, fast Fourier transform was performed to reach frequency domain data. It was assumed the transmitter, having TE-polarized field, to be in a distance of 10 m from the wall. The receiver/receivers were located at $x_m = 15$ cm in co-polarized mode. The wall with a permittivity of $\varepsilon_r = 4 + i0.1$ and a thickness of 30 cm was considered in a single-layered scenario. For further assessments, as illustrated in Fig. 2, a multilayered wall, including three and five layers with parameters listed in Tables I and II, was investigated. It was assumed the wall with constant parameters over 1–3 GHz to be located in a distance of $x_0 = 50$ cm from the receiver.

TABLE II
FIVE-LAYERED WALL PARAMETERS

Layers	type of layer	permittivity (ε)	conductivity σ (s/m)	thickness (cm)
1st layer	concrete	6.8	0.1	3
2nd layer	brick	2.3	0.03	10
3rd layer	air	1	0	5
4th layer	brick	2.3	0.03	10
5th layer	concrete	6.8	0.1	3

A. Incident Angle Effect

As could be seen from (5) and (6), the incident angle of the incident field is a factor of transmission coefficient, thereby affecting the target image in TWI, directly. Due to the fact that the illuminator of opportunity is in far-field and considered a plane wave illuminating the wall/target with its specific angle, the effect of incident angle should be investigated in PSAR-TWI, separately. In order to demonstrate the impact of incident angle on PSAR-TWI image, a single stationary plane wave with a frequency of 1–3 GHz, and a step of $\Delta f = 25$ MHz was assumed as an illuminator of opportunity. The transmitter was utilized in a number of incident angles for different wall-target scenarios. The image of targets was created using standard SAR imaging technique (3), which could mean that wall effects were not compensated thus wall parameters estimation was not necessary. SWR was calculated in terms of different wall-incident angle scenarios to show how the technique would suppress wall direct reflection. Furthermore, to validate and show the effectiveness of the technique, PSAR imaging results were compared with both well-known point source monostatic SAR and the TRM [28] applying free-space Green's function. The TRM is an approach to detect/image the target using an array of N transmitters/receivers antennas. Each antenna transmits a wave at a fixed frequency and the wave scattered from the medium is measured and registered at each antenna of the array. For TRM, the point at which maximum amplitude is observed will be the estimated position of the target.

As shown in (4), to construct an image behind a wall, transmission coefficient of the wall should be compensated. Apart from wall direct reflection which dominates the target, transmissivity is the key factor in TWI imaging results. It would change both the phase and amplitude of scattered signals. It should be noted that in the case of a point source, the transmissivity matrix would have different values, due to the different incident angles at any point of a target, hence dramatically degrades the target image. However, a plane wave transmitter would result in the same value of transmissivity matrix for all points. Therefore, at a fixed frequency, the effect of incident angle on reflection coefficient provides new insights into the way we investigate the incident angle effect on TWI image. In these regards, T and Γ of the mentioned single-layered wall for different θ_i are illustrated in Fig. 3(a) and (b), respectively. It could be seen that the minimum reflection, or maximum transmission coefficient, obtains at $\theta_i = 0°$. Also, the derivative of a transmission

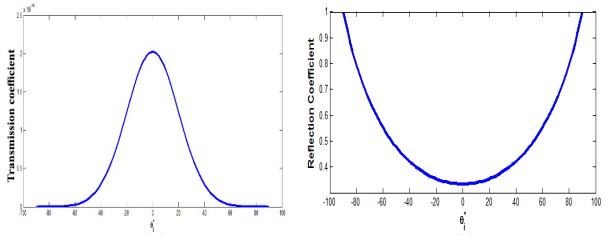

Fig. 3. (a) Wall transmission coefficient. (b) Wall reflection coefficient.

coefficient function with respect to θ_i, for a single layer (5) and multilayer [23], demonstrates that the maximum transmission through the wall would be obtained at $\theta_i = 0°$. It could be inferred that higher transmission coefficient is a result of a smaller incident angle and, conversely, in terms of reflection coefficient. Higher transmission coefficient or lower reflection led more waves to propagate through the wall, hence less reflection from the wall.

In the first example, a linear array receiver with 36 elements and 3.5-cm interlinear spacing would collect backscattered field from a circular PEC target. The target with a radius of 7.5 cm was centered at (175, 75) cm behind a single-layered wall. The imaging result of 0° incident angle illumination is drawn in Fig. 4(a) before subtracting the wall direct reflection or background subtraction. However, in the following results, the true region of the target was indicated with a black circle, rectangle, or ellipse. From the image, the target could be easily seen, with SWR equal to 4.68 dB, in addition to glints of the wall. As clear in Fig. 4(b), the target image was obtained at 30° transmitter, and the target could be easily detected. Wall direct signal was also obvious with SWR = 1.32 dB which was 3.36 dB less than 0° illumination. The imaging result of 45° illuminator is illustrated in Fig. 4(c), although the wall has higher density and SWR is −1.23 dB, the target can be observed. As can be noticed from Fig. 4, due to the lower wall transmissivity, bigger incident angle would result in lower SWR.

To verify the results, SAR and TRM images of the same scenery behind a single-layered wall are shown in Fig. 4(d) and (e), respectively, before background subtraction. For TRM, a number of 25 omnidirectional antennas simulated as point sources were used as an array for transceiver with the distance of 5 cm with each other. Also, the SAR scans the region of interest with 5-cm interelement spacing. As it is obvious in Fig. 4(d) and (e), since it was highly blurred and masked by the strong reflection of the wall, the target was not observable; while just the wall image can be seen which dominates the target image. It is worth mentioning that wall was the point at which maximum amplitude was observed, for TRM imaging result. On the other hand, in TWI-PSAR, because of the plane wave transmitter, all pixels of the scene would be illuminated by the same incident angle, with SWR not being too weak, where the target without background subtraction could be seen. However, for point source, none plane wave illuminator, each pixel tends to be illuminated with its own incident angle resulting different transmission coefficients for each pixel; thus, desired SWR might not be obtained for the target to be seen. It should be noticed that the difference in wave velocity between the free space and wall led to detecting the target relatively farther away from its actual location.

TABLE III
SWR IN MULTILAYERED WALL

	0° incident angle	20° incident angle	40° incident angle
Three layers	-0.93dB	-3.85dB	-3.21dB
Five layers	-3.35dB	-6.8dB	-7.01dB

For further assessment, multilayered wall was substituted for the single layer one in the previous example. SWR at all incident angles was calculated and summarized in Table III. The imaging results behind the three-layered wall are presented in Fig. 5, without background subtraction. Despite of the lower SWR than the same case in the single-layered wall, the target that illuminated at 0° could be recognized in Fig. 5(a). Because of the stronger wall reflection, the image was blurred, as shown in Fig. 5(b) and (c), at 20° and 40°, respectively. As depicted in Fig. 6, the same results could be obtained for the target behind the five-layered wall. Although the wall was made up of several layers, in addition to the dominated wall image, the faintest trace of target image could be seen at 0°, Fig. 6(a). As illustrated in Fig. 6(b) and (c), at 20° and 40°, respectively, the image could not be distinguished from other ghost images, and SWR was too low. As mentioned, it is primarily for these reasons that the transmission coefficient would decrease with growing angle and higher permittivity. The target with larger backscatter coefficient would be detected better than the smaller one. Therefore, in PSAR technique, transmitter with the incident angle around $\theta_i = 0°$ would mitigate wall effects more, without background subtraction and wall compensation. However, at other incident angles, wall direct reflection, because of the higher reflection coefficient, might dominate images, causing the target not to be identified correctly. To demonstrate the validity of the proposed method and make comparison, again, the imaging results of SAR and TRM behind the five-layered wall with the same scenery are presented in Fig. 6(d) and (e). The results are the same as Fig. 4, in which just the glint of the wall could be seen while it is not possible to see the target. Ultimately, these three examples confirm the fact that a target could be detected before background subtraction using PSAR, whereas SAR and TRM techniques, due to the target image being concealed under the wall, sound to be inefficient without background subtraction.

In the next two examples, the target of the previous scenery was investigated to show the effectiveness of the proposed method in terms of resolution, using free-space Green's function. Since SAR image could not be observed without background subtraction, the imaging results of Fig. 4 are presented in Fig. 7 after background subtraction for more precise comparison. Images of 0°, 30°, and 45° are shown in Fig. 7(a)–(c), respectively. Fig. 7(d) shows the SAR image after background

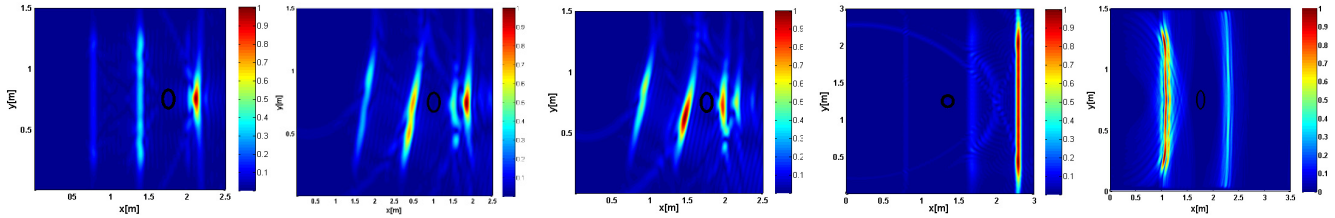

Fig. 4. Imaging results behind single-layered wall before background subtraction by PSAR illuminator at (a) 0°, (b) 30°, (c) 45°, (d) monostatic SAR, and (e) TRM.

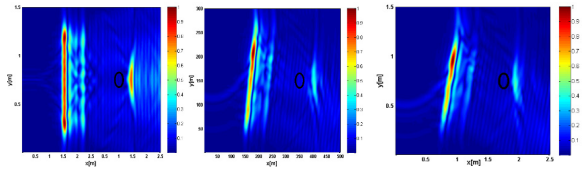

Fig. 5. Imaging results behind three-layered wall before background subtraction by PSAR illuminator at (a) 0°, (b) 20°, and (c) 40°.

subtraction. As clear in Fig. 7, using TWI-PSAR, the target could easily be recognized after background subtraction at all angles with a reasonable resolution. In contrast, because of the significant degradation in cross-range resolution, the target could not be identified in Fig. 7(d). This could mean that with a single incident angle, applying compensation technique (4) would not be needed. Consequently, TWI-PSAR, unlike other TWI methods requiring an efficient evaluation of the wall medium Green's function, has the capability of imaging by using free-space Green's function thus wall parameters could remain unknown. However, weak resolution in SAR necessitated wall compensation method requiring wall parameters to be known (4).

For multilayer cases, due to higher permittivity in five layers resulting in strong reflection, background subtraction seems essential. As stated, the strong wall reflection caused negative SWR. Although the target was observable, negative SWR could mean that the wall image tended to mask the target. Imaging results of the target behind the five-layered wall are shown in Fig. 8. It is clear, similar to Fig. 7, that the target image with a single incident angle (0°, 20°, and 40°, Fig. 8) could be perfectly detected. In this case, SAR significantly degrades the quality of images thus requiring wall compensation method. These results, again, demonstrate the superiority of the proposed TWI-PSAR method in terms of detecting and imaging the target without using background subtraction algorithms and wall compensation methods. However, in SAR, widening the target along the cross-range direction was observed, aside from the shift in the target position in the range direction. It should be pointed out that transmission coefficients, with different amplitudes and phases for each pixel, are the consequence of the point or none plane wave source used in SAR technique. Amplitude and phase of each pixel tend to influence on the target image differently. In other words, phase and amplitude of each pixel of the target vary with another one which results in widening the target along the cross-range direction. Therefore, wall medium Green's function is essential to compensate these changes in phase and amplitude, to compute the penetrated electromagnetic field correctly. Moreover, strong direct reflection of the wall, dominating the target image, would also necessitate background subtraction. However, in PSAR, wall direct reflections were strongly attenuated, especially in the vicinity of 0°, and the target was detectable without background subtraction. Because of the same transmissivity for all pixels, the same amplitude and phase for each pixel in the case of a plane wave transmitter, the resolution would not be degraded, thus, results would not need to be compensated. The only negative aspect of the uncompensated scenario in TWI-PSAR might be dislocation due to reducing wave velocity in the wall.

B. Target Detection in Multilayered Wall by Z-PSAR

Results show the main advantage of sources of opportunity with zero incident angle that would be a spurious signal reduction and an increase in SWR. As claimed, in cases where the incident angle is equal or near to zero, the target without background subtraction and wall compensation could be clearly identified. Z-PSAR would not only mitigate the wall effect, but, in conjunction with the monostatic SAR image, might also provide more detailed information of the target without background subtraction. Since in zero incident angle, transmission coefficient reaches its maximum point, the wave could have the best transmission through the wall.

Due to the distinctive features of Z-PSAR it could be widely used in TWI. In this case, regardless of the wall parameters and direct reflection, the target behind the wall could be imaged or tracked using a transmitter which illuminates the wall with normal incident angle. The geometry of Z-PSAR is depicted in Fig. 9.

As shown in Fig. 9, due to Snell's law and since in Z-PSAR the incident agle is $\theta_i = 0°$, the waves passing through the wall has the angle of $\theta_t = 0$. As a result, the normal component of the propagation constant in air, i.e., k_{0x}, would remain the same as wavenumber in free-space, i.e., k_0. Also, the normal component of the propagation constant in the wall, i.e., k_{1x}, would reach its maximum value, $k_{1\mathrm{x}} = k_0\sqrt{\varepsilon}\mathrm{r}$. Therefore, the minimum wall direct reflection and small changes in phase and amplitude of the scattered signals would be obtained. These results prove the distinctive feature of Z-PSAR in TWI. To evaluate Z-PSAR system and demonstrate its applicability

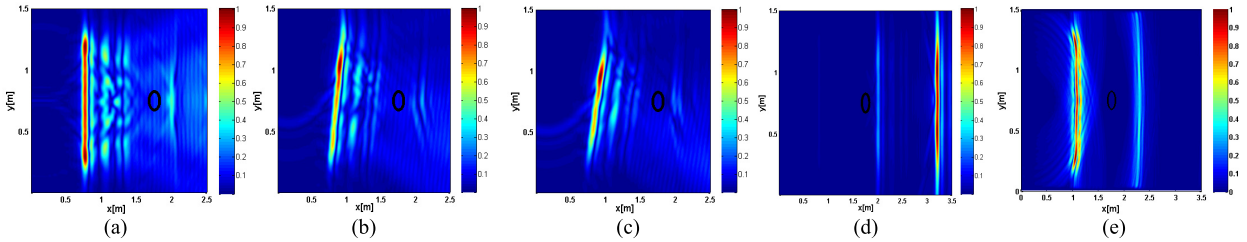

Fig. 6. Imaging results behind five-layered wall before background subtraction by PSAR illuminator at (a) 0°, (b) 20°, (c) 40°, (d) monostatic SAR, and (e) TRM.

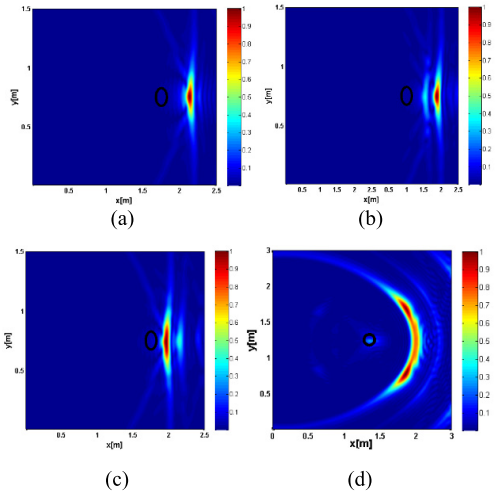

Fig. 7. Imaging results behind the single-layered wall after background subtraction at (a) 0° (b) 30° and (c) 45°, and (d) monostatic SAR.

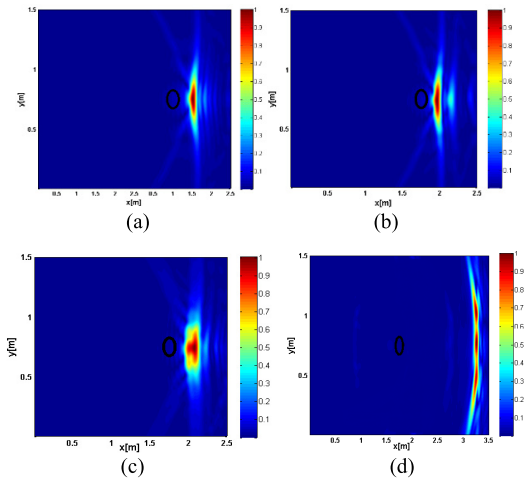

Fig. 8. Imaging results behind five-layered wall after background subtraction at (a) 0°, (b) 20° and (c) 40°, and (d) monostatic SAR.

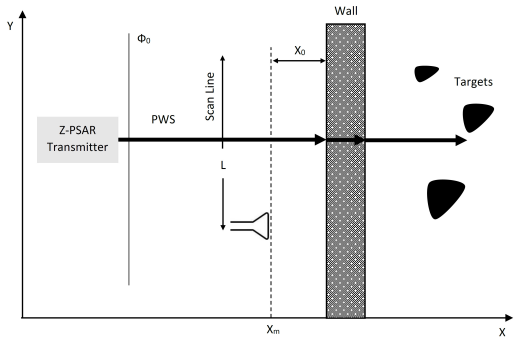

Fig. 9. Z-PSAR configuration.

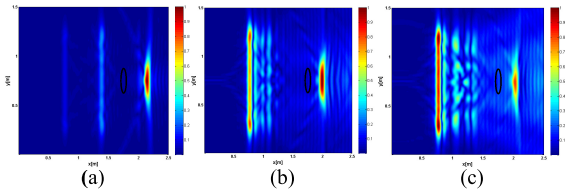

Fig. 10. Z-PSAR imaging results of a skin-like ellipse. (a) Behind single-layered wall. (b) Behind three-layered wall. (c) Behind five-layered wall.

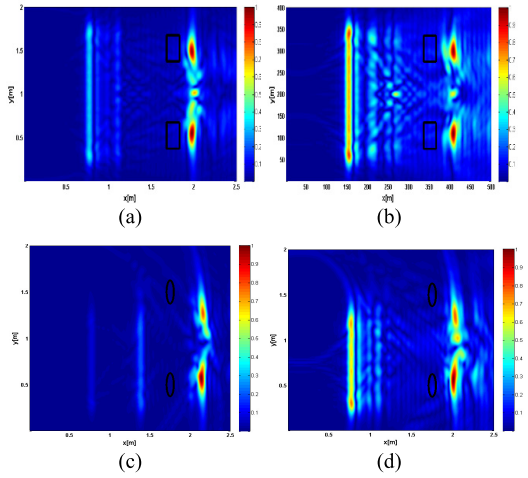

Fig. 11. Z-PSAR imaging results of two targets. (a) Rectangular PEC behind three-layered wall. (b) Rectangular PEC behind five-layered wall. (c) Skin-like ellipse behind single-layered wall. (d) Skin-like ellipse behind three-layered wall.

and usefulness, several Z-PSAR imaging results are presented using free-space Green's function (3) without background subtraction, in different wall-target scenarios. Targets under investigation were 15×30 cm^2 PEC rectangle. Also, to show simulations with more realistic targets, an elliptical shape with $a = 5$ cm, major radius, and $b = 3$ cm, minor radius, made to represent a 2-D section of humans, with skin-like parameters in terms of permittivity, $\varepsilon_r = 50$, and conductivity, $\sigma = 1$ S/m, [29] was used as the target to be imaged. First, the Z-PSAR imaging results of an ellipse, substituted for

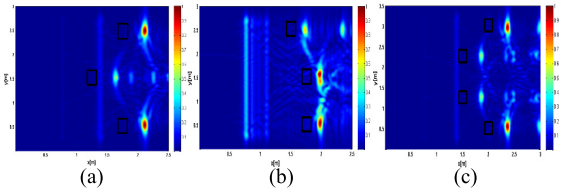

Fig. 12. Z-PSAR imaging results of (a) three targets behind single-layered wall, (b) three targets behind three-layered wall, and (c) four targets behind single-layered wall.

TABLE IV
TARGET POSITION

configuration	center position (cm)
three targets in single layered wall	target1: (175,50) target2: (125,150) target3: (175,250)
three targets in three - layered walls	target1: (175,50) target2: (175,150) target3: (150,250)
four targets in single layered wall	target1: (150,130) target2: (150,230) target3: (200,50 target4: (200,300)

the circular PEC target in the previous examples, are shown in Fig. 10. As clear in Fig. 10(a), Z-PSAR could image the skin-like target behind the single-layered wall easily. Moreover, its capability of imaging a skin-like target behind three and five-layered wall is obvious in Fig. 10(b) and (c), respectively. To show the capability of Z-PSAR in the presence of multitargets, the imaging results of two targets behind single- and multilayered wall are provided in Fig. 11. Z-PSAR receiver scanned the region of interest, synthesizing a 1.7-m aperture with 2-cm interelement spacing, with targets being located at (175, 50) cm, and (175,150) cm. Fig. 11(a) shows the PEC targets image behind the three-layered wall, being detected and identified correctly; just glint of the wall could be seen. The imaging results of two PEC targets behind the five-layered wall are drawn in Fig. 11(b). To investigate more deeply, the imaging results of two elliptical skin-like targets are presented in Fig. 11(c) and (d). As it is clear in Fig. 11(c), Z-PSAR could also image and detect two skin-like targets behind the single-layered wall. Again, in Fig. 11(d), the effectiveness of the Z-PSAR imaging behind the three-layered wall is confirmed that shows two elliptical skin-like targets were detected and shown.

For more complicated scenarios, the imaging results of three PEC targets are illustrated in Fig. 12(a) and (b) in single and three layers, respectively. Also, as illustrated in Fig. 12(c), four targets were detected easily using the Z-PSAR technique in which the receiver were moved along $L = 270$ cm, without using wall subtraction algorithms and compensation methods. The position of each target is summarized in Table IV. These results reexamined the capability of target detection behind the wall and verified that wall parameter estimation and subtraction methods are not necessary in Z-PSAR. However, from Fig. 12, it is clear that all targets could be located correctly; however, in the case of multitarget, the only negative

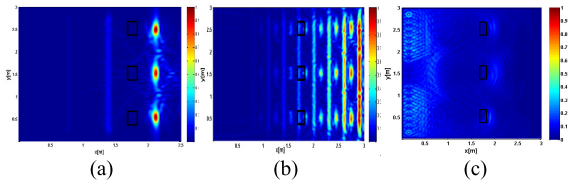

Fig. 13. Image of three targets behind single-layered wall by (a) Z-PSAR, (b) monostatic SAR, and (c) time reversal.

effect could be producing spurious peaks, called ghost targets. This is due to the fact that that the main advantage of illuminating the target at different incident angles is that a target can be observed from different bistatic angles, providing more information about the target. However, using a single transmitter located at 0° produced ghost targets mainly due to transmitters not being located at different observation points. Finally, to validate and show the robustness of the proposed technique, a comparison between Z-PSAR, SAR, and TRM are made. Three PEC targets were centered at (175, 50), (175,150), and (175,250), with the receiver collecting scattered signals similar to the previous case. For TRM, 27 antennas constructing an array of transceiver with the interelement spacing of 10 cm were used. As presented in Fig. 13(a), Z-PSAR has the capability to image and detect all three targets, correctly, besides wall negative effects suppression. Same as before, contrary to Z-PSAR, SAR and TRM are unable in imaging and detecting these three targets without background subtraction and wall compensation. SAR and TRM imaging results, using free-space Green's function, before wall reflection subtraction are illustrated in Fig. 13(b) and (c), respectively, in which targets are blurred and wall image dominates the targets. As obvious in Fig. 13(b), although resolution degraded, targets are not totally concealed and blurred in SAR. In fact, because of high reflection of the target, targets could also be seen along with wall image. The PEC targets, rectangular and bigger, in terms of size, than the circular one used in Section IV-A, result in higher reflection coefficient. However, since wall reflection still has the maximum amplitude, and due to the principle of TRM, maximum amplitude would be the estimated position, targets are not observable in Fig. 13(c).

Therefore, contrary to monostatic SAR and TRM, Z-PSAR demonstrated the ability not only to suppress the wall clutter but also to accurately detect and image several targets using free-space medium Green's function, proving the capability of imaging targets without using background subtraction algorithms and wall compensation methods. However, in monostatic SAR and TRM, wall clutter should be suppressed; otherwise, target detection would be difficult or impossible, especially for target with low reflectivity. In addition, other imaging methods require wall medium Green's function, a time consuming and difficult process, to image the target without any error.

C. Frequency Effect

As mentioned, frequency is considered one of the parameters affecting wall transmission coefficient directly. In the sections A, a single wideband stepped frequency plane wave

TABLE V
ILLUMINATOR PARAMETERS

Transmission	UHF TV (analogue)	Digital TV	Cellphone basestation (GSM)	Cellphone basestation (3G)	Global Positioning System(GPS)	Deep space radio communications	WiFi
Operating Frequency	550MHz	750MHz	900 MHz, 1.8 GHz	2GHz	1.227,1.575 GHz	2.29 GHz	2.2-3.5GHz
Incident Angle	30°	50°	60°	70°	45°	20°	0°
Polarization	horizontal	horizontal	circular	circular	circular	circular	Circular

transmitter was regarded as a source of illumination. In fact, to analyses the influence of incident angle on PSAR image in TWI, frequency image was fixed and assumed it is applicable to have a UWB stepped frequency transmitter of opportunity. However, in a real situation, it may not be possible to find a single stepped frequency as a source of opportunity with at least 1-GHz bandwidth and respectable power propagating through the wall as well. Moreover, in previous works in TWI [1]–[3] and [22], [23], it was common to use a source with the operating frequency with equally spaced frequency bins. Although a small step frequency could produce the image with high resolution, it is not required in every situation. From (2), P is the total number of frequencies and, thus, several transmitters with different frequencies can be integrated in order to make a wideband transmitter and to image a target with a proper resolution.

To achieve the required resolution, operation at high frequencies with a large frequency bandwidth provides the best results. However, the upper limit of frequency of operation is limited by attenuation through the materials. The required resolutions to detect human and other objects of same size are on the order of 10–15 cm. This corresponds to the usage of 1–1.5-GHz bandwidth at UHF to low microwave frequencies to provide the required range resolution. Thus, in TWI-PSAR, to obtain a reasonable resolution, it sounds necessary to select all transmitters of opportunity in the frequency range of 0.8–3.5 GHz, which could be integrated together and create a UWB transmitter. Consequently, the covered bandwidth would be written as: $\mathrm{BW} = f_{\max} - f_{\min}$, where $f_{\max}$ and $f_{\min}$ is the maximum and minimum frequency of sources, respectively. Therefore, because of the importance of frequency, which transmitters of opportunity should be used seem to be of paramount importance. Due to the fact that TWI-PSAR could play a crucial part in urgent situations, aside from frequency band and resulting bandwidth, the ubiquity of transmitters could be another effective factor in PSAR-TWI. Ultimately, it sounds logical to utilize sources such as commercial signals and GSM that are present everywhere, preferred in urgent conditions. In this section, commercial signals, such as TV, DVB-T, GSM, and WiMAX, were adopted as illuminators, with their parameters being listed in Table V. Since not all of these transmitters would illuminate the target with a single incident angle, wall effects need to be compensated. Thus, a generalized Green's function-based approach for imaging the targets behind a wall [23] is incorporated for the compensation

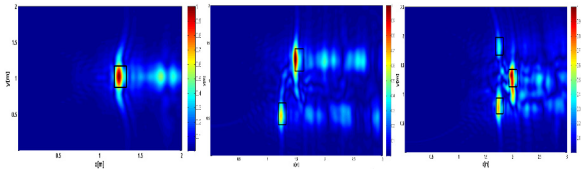

(a) (b) (c)

Fig. 14. Reconstructed image using commercial source behind the single-layered wall. (a) Single target. (b) Two targets. (c) Three targets.

of the wall effects. In these numerical simulations, wall parameters were assumed to be known. The interested readers were referred to [30] and [31] for the estimation of parameters for single- or multilayered wall using time and frequency domain methods.

In all following simulations, targets were rectangular PEC with 15×30 cm^2 dimensions. The analysis started using listed illuminators with a single rectangular target. The target was 70 cm away from the front boundary of the wall, and PSAR receiver moved along $L = 1.7$ m aperture with 0.02-m interelement spacing. Fig. 14(a) shows the reconstructed imaging result of adopted transmitter of opportunity. As can be seen, reconstructed image would possess reasonable resolution and locate the target correctly. However, the only negative effect of using transmitter of mentioned signals could be producing ghost targets. In the next two examples, results of multiple targets behind the wall were designed. Fig. 14(b) illustrates the reconstructed imaging result of two rectangles centered at (125, 50) cm and (150,125) cm, nearly close to each other, with PSAR receiver moving along $L = 1.7$ m aperture with a step of 2 cm. To verify the proposed method, a more complex scene, where three rectangles were centered at (175, 75), (200, 125), and (175, 175), was selected to be imaged; the reconstructed image is shown in Fig. 14(c). From Fig. 14, it is clear that all targets could be located correctly; however, in two or more relatively close targets, using transmitter of mentioned signals produced ghost targets mainly due to transmitters not being in a close frequency band.

It was observed that with commercial mission imaging in multitargets, some of the targets would not appear as sharp as the ones using stepped frequency transmitter in Section IV-B. Therefore, to create sharp image with commercial transmitters, it seemed necessary to adopt more transmitters in a close frequency that could cover whole band.

In addition to mentioned sources, numerous sources of opportunity, in the surrounding environment, which are in the

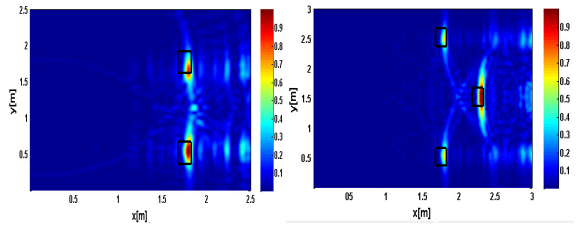

(a) (b)

Fig. 15. Reconstructed image using the Monte Carlo simulation 50 runs behind the single-layered wall. (a) Two targets. (b) Three targets.

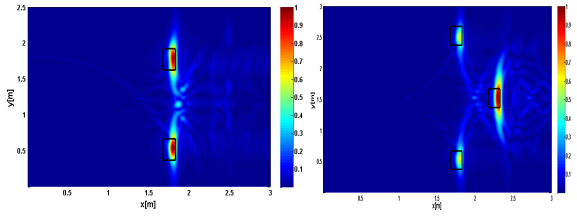

(a) (b)

Fig. 16. Reconstructed image using the Monte Carlo 200 simulation runs behind the single-layered wall. (a) Two targets. (b) Three targets.

desired TWI frequency band could be considered illuminators of opportunity in TWI-PSAR. To investigate more deeply, 25 sources with different frequency and incident angles, selected randomly, were used to analyses the TWI-PSAR performance.

To do so, the Monte Carlo method, the most used technique to obtain the statistical variation and known as gold standard of statistical simulations [32], was used. The result of the Monte Carlo simulation with 50 FDTD runs is shown in Fig. 15. PSAR receiver moves along $L = 220$ cm with a step of 2 cm. Fig. 15(a) shows the imaging result of two targets centered at (175, 50) cm and (175,175) cm. Another simulation was performed for imaging three targets located at (175, 50) cm, (175,220) cm, and (225,150) cm, presented in Fig. 15(b). As it can be seen from Fig. 15, the targets are clearly detected with less ghost image in comparison with the previous examples.

For further assessments, the Monte Carlo simulations with 200 FDTD runs were performed for the previous examples (Fig. 16). Compared with Fig. 15, it is obvious that the more Monte Carlo simulation runs would result in the cleared image with less ghost image. This is primarily because of the fact that in the case of using more randomly selected frequencies and incident angles, the possibility to cover more frequency bands, and the probability of observing the target in more incident angles would increase.

V. Conclusion

A passive SAR technique, namely, TWI-PSAR, was introduced and used to image targets behind single-/multilayered walls using transmitters of opportunity, and a receiver that could be mounted on a moving platform or fixed as an array antenna. This technique proved potential and promising applications in reducing the complexity and cost of TWI radar with a proper performance. Since wall transmissivity is considered a function of incident angles, the effect of the wall on the target image would be significant. Basically, the cross-range resolution tends to be degraded if the standard SAR imaging is applied. Instead, a wideband stationary transmitter with a single incident angle was proposed to mitigate the effect of walls, and the focused target image was nearly obtained before wall compensation. When background measurement might not be available, with wall parameters being unknown for image reconstruction, a transmitter of opportunity with Z-PSAR could be adopted as a wall mitigation technique to remove wall effects. The simulation results showed that the proposed method would mitigate wall effects, and targets could be identified without background subtraction and wall compensation. The proposed technique can provide high-quality focused image in a short computation time regardless of the estimated value of the wall parameters, using free-space Green's function. TWI-PSAR was compared with the monostatic SAR and the TRM, requiring wall medium Green's function, where wall effects should be compensated and wall direct reflection should be subtracted. Furthermore, in a real situation where a wideband stepped frequency is not available, the new method would also be able to image and identify targets by integrating several transmitters of opportunity, such as DAB radio, DVB-T television, GSM mobile system, and Wi-Fi to form wideband source. In addition to the mentioned sources, several sources, selected randomly, were used in Monte Carlo Simulations. Focused imaging results were achieved due to the incorporation of layered medium Green's function that would fully take into account and compensate for wall effects. Therefore, PSAR showed the ability not only to suppress wall effects but also to accurately locate and image targets using transmitters of opportunity.

Acknowledgment

This research did not receive any specific grant from funding agencies in the public, commercial, or not-for-profit sectors.

References

[1] F. Ahmad, M. G. Amin, S. A. Kassam, and G. J. Fraze, "A wideband, synthetic aperture beamformer for through-the-wall imaging," in *Proc. IEEE Int. Symp. Phased Array Syst. Technol.*, Oct. 2003, pp. 187–192.

[2] M. Dehmollaian and K. Sarabandi, "Refocusing through building walls using synthetic aperture radar," *IEEE Trans. Geosci. Remote Sens.*, vol. 46, no. 6, pp. 1589–1599, Jun. 2008.

[3] T. Dogaru and C. Le, "SAR images of rooms and buildings based on FDTD computer models," *IEEE Trans. Geosci. Remote Sens.*, vol. 47, no. 5, pp. 1388–1401, May 2009.

[4] R. Solimene, F. Soldovieri, G. Prisco, and R. Pierri, "Three-dimensional through-wall imaging under ambiguous wall parameters," *IEEE Trans. Geosci. Remote Sens.*, vol. 47, no. 5, pp. 1310–1317, May 2009.

[5] W. Zhang, A. Hoorfar, and C. Thajudeen, "Building layout and interior target imaging with SAR using an efficient beamformer," in *Proc. APSURSI*, Jul. 2011, pp. 2087–2090.

[6] W. Zhang, A. Hoorfar, C. Thajudeen, and F. Ahmad, "Full polarimetric beam-forming algorithm for through-the-wall radar imaging," *Radio Sci.*, vol. 46, no. 5, pp. 1–17, Oct. 2011.

[7] W. Zhang and A. Hoorfar, "Three-dimensional synthetic aperture radar imaging through multilayered walls," *IEEE Trans. Antennas Propag.*, vol. 62, no. 1, pp. 459–462, Jan. 2014.

[8] G. Krieger and A. Moreira, "Multistatic SAR satellite formations: Potentials and challenges," in *Proc. IGARSS*, Jul. 2005, pp. 2680–2684.

[9] L. M. H. Ulander and T. Martin, "Bistatic ultra-wideband SAR for imaging of ground targets under foliage," in *Proc. IEEE Int. Radar Conf.*, May 2005, pp. 419–423.
[10] G. Yates, A. M. Home, A. P. Blake, and R. Middleton, "Bistatic SAR image formation," *IEE Proc.-Radar, Sonar Navigat.*, vol. 153, no. 3, pp. 208–213, Jun. 2006.
[11] D. Gromek, K. Kulpa, and P. Samczyński, "Experimental results of passive SAR imaging using DVB-T illuminators of opportunity," *IEEE Geosci. Remote Sens. Lett.*, vol. 13, no. 8, pp. 1124–1128, Aug. 2016.
[12] C. C. H. Yardley, "Passive bistatic radar based on target illuminations by digital audio broadcasting," *IET Radar Sonar Navigat.*, vol. 2, no. 5, pp. 366–375, Oct. 2008.
[13] Z. Zeng, "Generic signal synchronisation algorithm for passive global navigation satellite system-based synthetic aperture radar," *IET Radar Sonar Navigat.*, vol. 9, no. 4, pp. 364–373, Apr. 2015.
[14] S. R. Stevens and J. A. Jackson, "Emitter selection criteria for passive multistatic synthetic aperture radar imaging," *IET Radar Sonar Navigat.*, vol. 8, no. 9, pp. 1267–1279, Dec. 2014.
[15] C. E. Yarman and B. Yazici, "Synthetic aperture hitchhiker imaging," *IEEE Trans. Image Process.*, vol. 17, no. 11, pp. 2156–2173, Nov. 2008.
[16] S. Reuter, F. Behner, H. Nies, O. Loffeld, D. Matthes, and J. Schiller, "Development and experiments of a passive SAR receiver system in a bistatic spaceborne/stationary configuration," in *Proc. IEEE Int. Geosci. Remote Sens. Symp. (IGARSS)*, Jul. 2010, pp. 118–121.
[17] L. Li, W. Zhang, and F. Li, "A novel autofocusing approach for real-time through-wall imaging under unknown wall characteristics," *IEEE Trans. Geosci. Remote Sens.*, vol. 48, no. 1, pp. 423–431, Jan. 2010.
[18] C. Zhang, Y. Kuga, and A. Ishimaru, "Hard-wall radar imaging: Localization of objects shadowed by metallic walls with MIMO radar," *IEEE Trans. Antennas Propag.*, vol. 66, no. 8, pp. 4240–4251, Aug. 2018.
[19] F. H. C. Tivive, A. Bouzerdoum, and M. G. Amin, "An SVD-based approach for mitigating wall reflections in through-the-wall radar imaging," in *Proc. IEEE Radar Conf. (RADAR)*, May 2011, pp. 519–524.
[20] Y. Yeo-Sun and M. G. Amin, "Spatial filtering for wall-clutter mitigation in through-the-wall radar imaging," *IEEE Trans. Geosci. Remote Sens.*, vol. 47, no. 9, pp. 3192–3208, Sep. 2009.
[21] F. Fioranelli, S. Salous, and X. Raimundo, "Frequency-modulated interrupted continuous wave as wall removal technique in through-the-wall imaging," *IEEE Trans. Geosci. Remote Sens.*, vol. 52, no. 10, pp. 6272–6283, Oct. 2014.
[22] M. Dehmollaian, M. Thiel, and K. Sarabandi, "Through-the-wall imaging using differential SAR," *IEEE Trans. Geosci. Remote Sens.*, vol. 47, no. 5, pp. 1289–1296, May 2009.
[23] W. Zhang and A. Hoorfar, "A generalized approach for SAR and MIMO radar imaging of building interior targets with compressive sensing," *IEEE Antennas Wireless Propag. Lett.*, vol. 14, pp. 1052–1055, 2015.
[24] R. G. Wiley, *ELINT: The Interception and Analysis of Radar Signals*, vol. 685. Boston, MA, USA: Artech House, 2006.
[25] K. Kulpa, "The CLEAN type algorithms for radar signal processing," in *Proc. IEEE MRRS*, Sep. 2008, pp. 152–157.
[26] K. Kulpa, P. Samczynski, M. Malanowski, L. Maslikowski, and V. Kubica, "The use of CLEAN processing for passive SAR image creation," in *Proc. IEEE RADAR*, Apr./May 2013, pp. 1–6.
[27] J. A. Kong, *Electromagnetic Wave Theory*. Cambridge, MA, USA: EMW Publishing, 2000.
[28] M. Fink *et al.*, "Time-reversed acoustics," *Rep. Prog. Phys.*, vol. 63, no. 12, pp. 1933–1999, 2000.
[29] T. Dogaru and C. Lee, "Simulated radar range profiles of a simple room as compound by FDTD and Xpatch," Army Res. Lab., Adelphi, MD, USA, Tech. Rep. ARL-TR-4420, 2008.
[30] C. Thajudeen, A. Hoorfar, and W. Zhang, "Estimation of frequency-dependent parameters of unknown walls for enhanced through-the-wall imaging," in *Proc. IEEE APS/URSI Conf.*, Spokane, WA, USA, Jul. 2011, pp. 3070–3073.
[31] M. Aftanas, "Through wall imaging with UWB radar system," Ph.D. dissertation, Faculty Elect. Eng. Inform., Tech. Univ. Košice, Košice, Slovakia, 2009.
[32] M. N. O. Sadiku, *Monte Carlo Methods for Electromagnetics*. Boca Raton, FL, USA: CRC Press, 2009.

Hajar Abedi was born in Savadkuh, Iran, in 1991. She received the B.Sc. and M.Sc. degrees in electrical engineering from the Babol Noshirvani University of Technology, Babol, Iran, in 2014 and 2017, respectively.

She is currently a Research Assistant with the Antenna and Microwave Laboratory, Babol Noshirvani University of Technology. Her research interests include radar and sonar systems, numerical methods in electromagnetics electromagnetic wave propagation, scattering, microwave imaging, and inverse scattering.

Bijan Zakeri (M'15) was born in Babol, Iran, in 1974. He received the M.Sc. and Ph.D. degrees in electromagnetics engineering from the Amirkabir "Polytechnic" University of Technology, Tehran, Iran, in 1999 and 2007, respectively.

In 2011, he became the Head of the joint research project entitled "RCS, IR, and Acoustic Signature Reduction of Surface Ships" with Iran Marine Industries Organization, Isfahan, Iran, and the Babol Noshirvani University of Technology, Babol. Since 2013, he has been an Associate Professor with the Electrical Engineering Department, Babol Noshirvani University of Technology, where he is also the Director of the Antenna and Microwave Laboratory and the Head of the Radar Research Team. His research interests include the application of electromagnetic numerical techniques in solving radiation and scattering problems, radar microwave subsystems, ultra-wideband antenna, and Polin-synthetic aperture radar remote sensing.

Dr. Zakeri is currently a member of the Iranian Association of Information and Communication Technology.